Patterns of the Aharonov-Bohm oscillations in graphene nanorings

Igor Romanovsky,* Constantine Yannouleas,† and Uzi Landman‡
School of Physics, Georgia Institute of Technology, Atlanta, Georgia 30332-0430, USA
(Received 2 December 2011; revised manuscript received 3 April 2012; published 17 April 2012)

Using extensive tight-binding calculations, we investigate (including the spin) the Aharonov-Bohm (AB) effect in monolayer and bilayer trigonal and hexagonal graphene rings with zigzag boundary conditions. Unlike the previous literature, we demonstrate the universality of integer (hc/e) and half-integer ($hc/2e$) values for the period of the AB oscillations as a function of the magnetic flux, in consonance with the case of mesoscopic metal rings. Odd-even (in the number of Dirac electrons, N) sawtooth-type patterns relating to the halving of the period have also been found; they are more numerous for a monolayer hexagonal ring, compared to the cases of a trigonal and a bilayer hexagonal ring. Additional, more complicated patterns are also present, depending on the shape of the graphene ring. Overall, the AB patterns repeat themselves as a function of N, with periods proportional to the number of the sides of the rings.

DOI: 10.1103/PhysRevB.85.165434 PACS number(s): 73.23.−b, 73.22.Pr

I. INTRODUCTION

Due to the widespread interest in nanoscience and nanotechnology in the past 15 years, persistent currents (PCs) and the Aharonov-Bohm (AB) effect in ring-type nanosystems have attracted much attention. Originally, PCs and the AB effect were studied theoretically for spinless electrons in the ideal case of strictly one-dimensional (1D; zero-width) metallic nanorings threaded by a solenoidal magnetic flux.[1–4] Subsequently, consideration of spin in this ideal case was shown[5] to lead to a nontrivial odd-even behavior, associated with halving ($\Phi_0/2$ versus Φ_0) of the universal AB period and of the corresponding amplitude of the AB oscillations as a function of the applied magnetic field B; $\Phi_0 = hc/e$ is the unit of magnetic flux.

Recently fabricated new carbon-based materials, like carbon nanotubes[6] and two-dimensional graphene, provide additional opportunities for investigations of PCs and the AB effect, with potential future technological applications, in ring-type nanodevices. However, despite the recent extraordinary interest in graphene (starting with the isolation of a single graphene sheet),[7] only a few experimental[8,9] and theoretical studies (see, e.g., Refs. 10–13) of PCs and the AB effect in graphene nanorings have appeared in the last couple of years. Surprisingly, these graphene-ring studies have been inconclusive regarding the aforementioned odd-even behavior associated with the electron spin; at the same time, no regular behavior or other pattern of the AB oscillations was reported. Moreover, one[11] of these publications has concluded that the odd-even behavior fails to manifest in graphene nanorings at all.

In this paper, based on extensive tight-binding (TB) calculations, we investigate AB oscillations for the case of trigonal and hexagonal narrow graphene rings terminating in zigzag edges; for experimental advances in the fabrication of graphene samples with well-defined high-purity edges, see Ref. 14. Our systematic studies (in the size range $1 \leqslant N \leqslant 100$ Dirac electrons) reveal clear signatures of several well-defined patterns (including odd-even and halved-period behaviors) that can be traced to consideration of both the spin degree of freedom and the zigzag boundary conditions obeyed by graphene Dirac electrons. The different conclusion arrived at in this article in comparison with previous publications[10,11] appears to be due to the simplified[15] condition (infinite-mass boundary condition, which, unlike the zigzag condition, cannot describe different crystallographic terminations and corner geometries in graphene) used in the latter, in conjunction with the circular symmetry required for obtaining analytic solutions of the continuous Dirac-Weyl equation.

II. PRELIMINARY THEORETICAL BACKGROUND

The spectra of an ideal metallic ring[3] (IMR) are very regular, exhibiting a parabolic dependence on the magnetic flux Φ, which is portrayed by the simple analytic expression

$$\varepsilon_i^{\mathrm{IMR}}(\Phi) \propto (l - \Phi/\Phi_0)^2, \tag{1}$$

where the single-particle angular momentum l takes the values $l = 0, \pm 1, \pm 2, \ldots$. This regularity is directly reflected in AB-related quantities, such as the persistent current I and the total magnetization M, which exhibit a periodic behavior as a function of Φ with period Φ_0 (for spinless electrons[3]) or both Φ_0 and $\Phi_0/2$ (when the electron spin is considered).[5] Indeed, one has

$$I = -c\frac{dE_{\mathrm{tot}}}{d\Phi} \quad \text{and} \quad M = -\frac{dE_{\mathrm{tot}}}{dB}, \tag{2}$$

where the total energy

$$E_{\mathrm{tot}} = \sum_{i,\sigma}^{\mathrm{occ}} \varepsilon_i(B) \tag{3}$$

is given by the sum over all occupied single-particle (noninteracting electron)[16] energies; the index σ runs over spins. The magnetic flux in Eq. (2) is specified as $\Phi = BS$, where the area $S = \pi R^2$, with R being the radius of the 1D ideal ring; for advances in the measurement of small PCs and magnetic moments, see Ref. 14(b).

To determine the single-particle spectrum [energy levels $\varepsilon_i(B)$] in the TB calculations for graphene rings, we use the Hamiltonian

$$H_{\mathrm{TB}} = -\sum_{\langle i,j \rangle} t_{ij} c_i^\dagger c_j + \mathrm{H.c.}, \tag{4}$$

with the angle braces indicating summation over the nearest-neighbor sites i, j. The hopping matrix element

$$t_{ij} = t \exp\left(\frac{ie}{\hbar c}\int_{\mathbf{r}_i}^{\mathbf{r}_j} d\mathbf{s}\cdot\mathbf{A}(\mathbf{r})\right), \quad (5)$$

where $t = 2.7$ eV, $\mathbf{r}_i$ and $\mathbf{r}_j$ are the positions of the carbon atoms i and j, respectively, and $\mathbf{A}$ is the vector potential associated with the applied perpendicular magnetic field B. The diagonalization of the TB Hamiltonian Eq. (4) is implemented with the use of the sparse-matrix solver ARPACK.[17] In calculating $E_{\rm tot}$ [see Eq. (2)], only single-particle TB energies with $\varepsilon_i(B) > 0$ are considered.[10,11] We note here that, unlike the continuous Dirac-Weyl equations,[10,11] both the K and the K' valleys are automatically incorporated in the TB treatment of graphene nanorings.

III. MONOLAYER TRIGONAL RING

First, we analyze TB results for a narrow trigonal graphene ring having pure zigzag terminations for both the inner and the outer edges [see Fig. 1(a)]. The corresponding TB spectra are displayed in Fig. 2(a). Since the constant magnetic field B is applied across the whole width of the ring, the magnetic flux is defined here in an average sense, i.e., through the use of an average area $S_{\rm av}$ given by

$$S_{\rm av} \approx (S_{\rm inn} + S_{\rm out})/2, \quad (6)$$

where the indices "inn" and "out" indicate the areas enclosed by the inner and outer edges of the ring, respectively.

The graphene-ring spectra in Fig. 2(a) are different from the simple spectra in Eq. (1), familiar from the case of 1D metallic rings.[3] Specifically, they are grouped in bunches of six levels (see also Ref. 18), and each such bunch contains two three-level units. Naturally, this organization is reflected in the behavior of the AB oscillations. Indeed, we found that the AB oscillations for the magnetization $M(\Phi)$ exhibits an overall period of $2 \times 6 = 12$ as a function of the electron number N (the factor of 2 resulting from the spin degree of freedom). Within this period of 12 electrons, we find four distinct patterns as a function of Φ (see Fig. 3), namely, (a) sawtooth, (b) pinched sawtooth, (c) asymmetric rounded sawtooth, and (d) halved-period sawtooth.

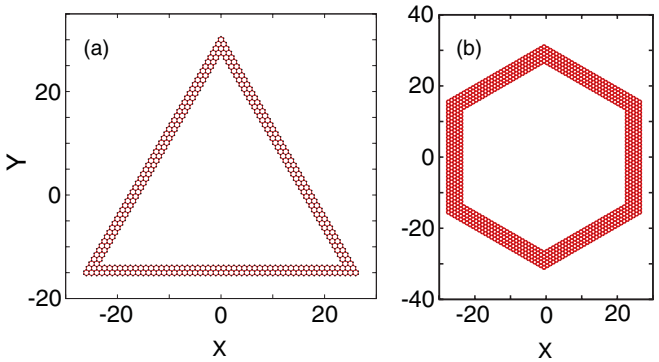

FIG. 1. (Color online) Diagram of narrow trigonal and hexagonal graphene rings with zigzag boundary conditions (for both the inner and the outer edges) used in TB calculations. (a) Equilateral trigonal ring with a width of three rows of carbon atoms; (b) hexagonal ring (with edges forming concentric regular polygons) with a width of five rows. The length unit is the lattice constant $a = 0.246$ nm.

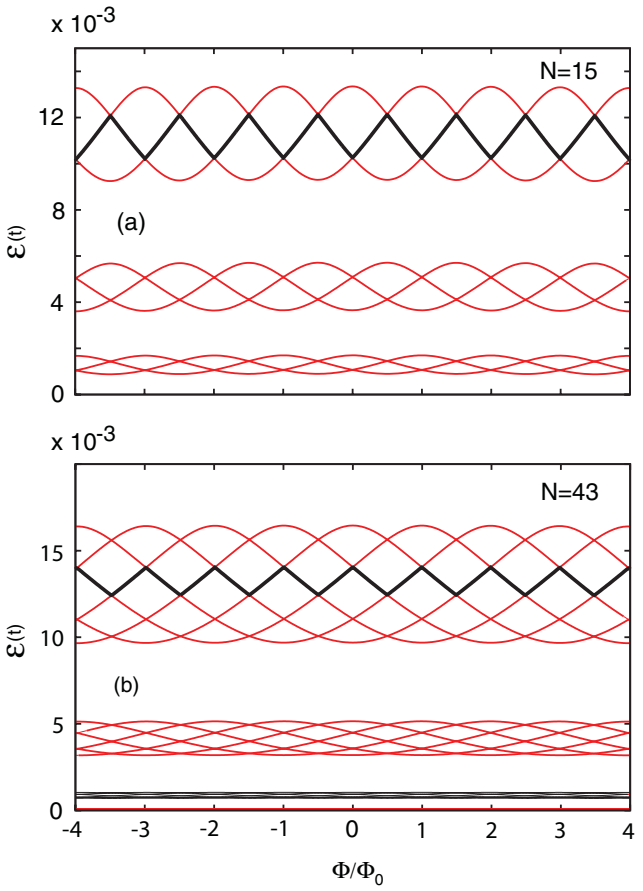

FIG. 2. (Color online) Characteristic TB low-energy spectra of the narrow graphene rings with zigzag boundary conditions portayed in Fig. 1. (a) Trigonal graphene ring; (b) hexagonal graphene ring. Thick black lines indicate the highest occupied state for $N = 15$ (a) and $N = 43$ (b) Dirac electrons (spin included). Note the threefold energy bands for the trigonal ring in (a) and the sixfold ones for the hexagonal ring in (b). In the case of the trigonal ring (odd number of sides), the consecutive threefold bands are shifted by a phase $\Phi_0/2$ with respect to each other; this results in a doubling of the period of the AB patterns as a function of N, i.e., a period of 12 instead of 6 (spin included). In the case of the hexagonal-ring spectrum (even number of sides), no such shift is present, and the period as a function of N remains 12 (spin included).

The first three patterns [Figs. 3(a)–3(c)] exhibit a period of Φ_0 as a function of Φ, while the fourth pattern [Fig. 3(d)] has a halved period $\Phi_0/2$. As mentioned, the halving of the fundamental period Φ_0 was seen earlier in studies[5] of the AB effect for spinfull electrons in ideal 1D metallic rings. In this case, it was described as an odd-even effect due to a two-electron alternation as a function of N. In contrast, the halving of the fundamental period in the case of trigonal graphene nanorings exhibits a six-electron period as a function of N, namely, for $N = 6i + N_0$, and only when $N_0 = 3$ ($i = 1,2,\ldots$).

Another regular behavior in the AB patterns of trigonal graphene rings is a constant shift of the Φ dependence by $\pm\Phi_0/2$ for all electron sizes related by $N = 6i + N_0$, with

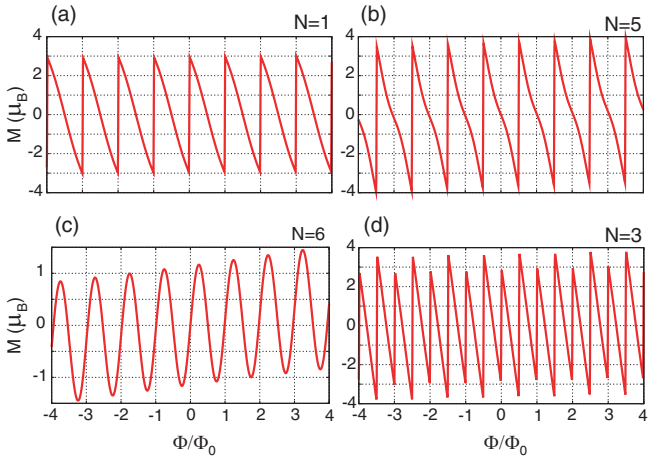

FIG. 3. (Color online) Magnetization as a function of the the magnetic flux Φ (spin is included). The four characteristic patterns of the Aharonov-Bohm oscillations associated with a trigonal graphene ring having zigzag boundary terminations [see Fig. 1(a)] are portrayed: (a) sawtooth; (b) pinched sawtooth; (c) asymmetric rounded sawtooth; (d) halved-period sawtooth.

$N_0 = 1,2,\ldots,6$; N_0 is kept constant while i runs over $i = 1,2,3,\ldots$. For example, the pattern of $N = 8$ is the same as that of $N = 2$, but shifted by $\Phi_0/2$, and the same holds for the pattern of $N = 10$ relative to that of $N = 4$, etc.

Taking consideration of the above, and through inspection of magnetization curves in the range $1 \leqslant N \leqslant 100$, the following summary of AB patterns can be deduced ($i = 1,2,\ldots$):

(1) Sawtooth pattern (a) with zero shift: $N = 12i + 1$, $N = 12i + 2$, $N = 12i + 10$.

(2) Sawtooth pattern (a) with a $\Phi_0/2$ shift: $N = 12i + 4$, $N = 12i + 7$, $N = 12i + 8$.

(3) Pinched sawtooth pattern (b) with a $\Phi_0/2$ shift: $N = 12i + 5$.

(4) Pinched sawtooth pattern (b) with zero shift: $N = 12i + 11$.

(5) Asymmetric rounded sawtooth pattern (c) with zero shift: $N = 12i + 6$.

(6) Asymmetric rounded sawtooth pattern (c) with a $\Phi_0/2$ shift: $N = 12i + 12$.

(7) Halved-period sawtooth pattern (d) with zero shift: $N = 12i + 3$.

(8) Halved-period sawtooth pattern (d) with a $\Phi_0/2$ shift: $N = 12i + 9$.

To summarize, $\Phi_0/2$ oscillations as a function of the magnetic flux occur only in cases 7 and 8, with the latter also involving an overall $\Phi_0/2$ shift.

IV. MONOLAYER HEXAGONAL RING

Next we analyze AB oscillations in the case of a narrow hexagonal graphene ring with zigzag edges [see Fig. 1(b)]. The corresponding energy spectrum [see Fig. 2(b)] again exhibits an organization in bands, as was the case with the spectra of the trigonal ring. However, each band now contains six, instead of three, single-particle levels, and this is clearly connected to the sixfold point-group symmetry of the regular hexagon (the three-level bands arising also from the threefold symmetry of the equilateral triangle).

Compared to the trigonal-ring spectra, the hexagonal-ring spectra are simpler in one way; namely, there is no phase shift between two successive sixfold bands [see Fig. 2(b)], in contrast to the $\Phi_0/2$ shift between successive threefold bands for the trigonal rings [see Fig. 2(a)]. The presence (absence) of a $\Phi_0/2$ shift between successive bands appears to be a general behavior of the spectra of regular-polygon-shaped graphene rings with an odd (even) number of sides.

The absence of a shift between consecutive energy bands leads to a simplification of the AB patterns, since it results in a period of $2 \times 6 = 12$ (avoiding the doubling to 24) electrons as a function of N. Of particular interest is the fact that, disregarding a potential shift of $\pm\Phi_0/2$, the AB patterns exhibited by the magnetization curves (see Fig. 4) display a well-developed (although apparently not perfect) alternation pattern between integer periods (Φ_0) and halved periods ($\Phi_0/2$), as long as the highest occupied state lies in the interior of the sixfold energy band. The $\Phi_0/2$ period reflects the zigzag nature of the interior states (which we term W states to distinguish from the zigzag boundary condition); examples of W states are given by the thick black lines in Fig. 2. When the Fermi level (highest occupied state) coincides with a

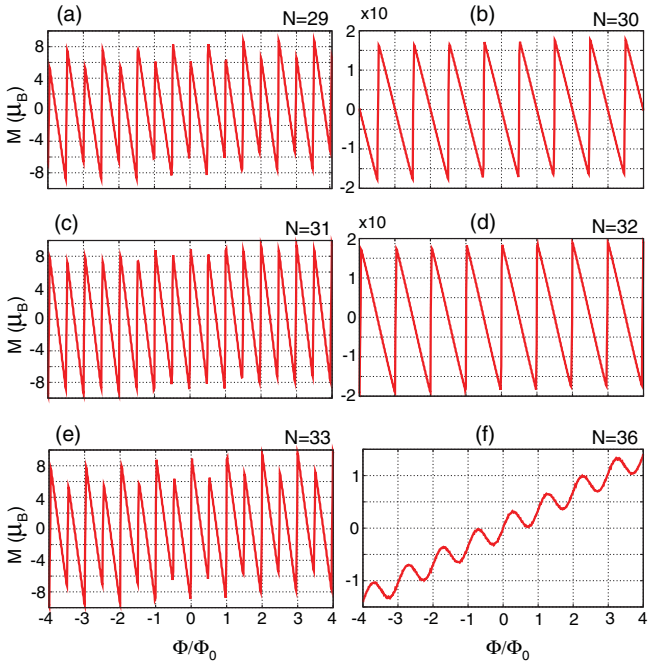

FIG. 4. (Color online) Magnetization as a function of the the magnetic flux Φ (spin is included). Six patterns of the Aharonov-Bohm oscillations associated with a hexagonal graphene ring having zigzag boundary terminations [see Fig. 1(b)] are portrayed. The first five patterns (a)–(e) correspond to single-particle states near the middle of the 12-fold spectral band (spin included), while the sixth pattern (f) corresponds to the top state [see Fig. 2(b)]. (a) $N = 29$; shifted halved-period sawtooth pattern. (b) $N = 30$; shifted sawtooth pattern. (c) $N = 31$; halved-period sawtooth pattern. (d) $N = 32$; sawtooth pattern. (e) $N = 33$; halved-period sawtooth pattern. (f) $N = 36$; rounded sawtooth pattern. (a)–(e) The qualitative development of an odd-even alternation between one-period, Φ_0, and halved-period, $\Phi_0/2$, sawtooth patterns is evident.

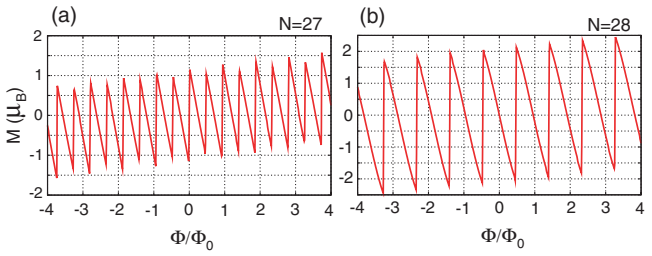

FIG. 5. (Color online) Patterns of Aharonov-Bohm oscillations associated with a wider [in comparison with Fig. 1(b)] hexagonal monolayer graphene ring (with 12 rows of carbon atoms on each side) having zigzag boundary terminations. (a) $N = 27$; halved-period sawtooth. (b) $N = 28$; sawtooth.

W state, $\Phi_0/2$ oscillations occur. Note that there are four W states for the hexagonal ring, but only one W state for the trigonal ring.

In Fig. 4, we display the magnetization curves for several instances of electrons occupying states in the 12-fold band with a number of electrons ranging from $N = 25$ to $N = 36$ (the doubling $2 \times 6 = 12$ is due to consideration of the electron spin). In the range $27 \leqslant N \leqslant 34$, the magnetization curves exhibit an odd-even effect associated with the alternation between a whole-period (Φ_0) sawtooth oscillation and a halved-period ($\Phi_0/2$) sawtooth pattern *(exhibiting also a halved amplitude)*; examples of this behavior are portrayed in Figs. 4(a)–4(e). The two cases for $N = 25$ and $N = 26$, with the 25th and 26th electrons occupying the bottom level of the sixfold band, both exhibit a full-period (Φ_0) sawtooth behavior. Finally, the two electrons occupying the top level of this energy band (corresponding to $N = 35$ and $N = 36$) exhibit a dissimilar behavior, with the penultimate one ($N = 35$) having a full-period (Φ_0) sawtooth behavior and the ultimate one ($N = 36$) showing a full-period (Φ_0) rounded-sawtooth behavior [see Fig. 4(f)]. Naturally, the aforementioned AB patterns repeat themselves with a period of 12 electrons.

In Fig. 5, we display illustrative magnetization curves for the case of a wider hexagonal ring compared to the one in Fig. 1(b) (by a factor of 2.4). From an inspection of the patterns in Fig. 5, as well as others not shown here, we found that the behavior of the AB oscillations in this wider ring changes only in minor ways. Much wider rings are needed to reach a substantial modification in the AB behavior.

V. SIMILARITIES TO THE IDEAL METAL RING

To gain further insight into the appearance of the odd-even AB behavior in graphene nanorings with zigzag terminations (described in Secs. III and IV), we plot in Fig. 6 the total energy curves, $E_{\rm tot}(\Phi)$ [see Eq. (3)], as a function of the average magnetic flux Φ [see Eq. (6)] for two characteristic cases, namely, $N = 30$ and $N = 31$, discussed earlier for an hexagonal graphene ring [see Figs. 4(b) and 4(c)].

A remarkable feature of these total energy curves is the almost-parabolic ($\propto\Phi^2$) dependence on the magnetic flux (equivalently the applied magnetic field), which exhibits a period Φ_0 for $N = 30$ (even) and a half-period $\Phi_0/2$ for $N = 31$ (odd). The odd-even sawtooth oscillations of the magnetization portrayed in Fig. 4 are a direct consequence

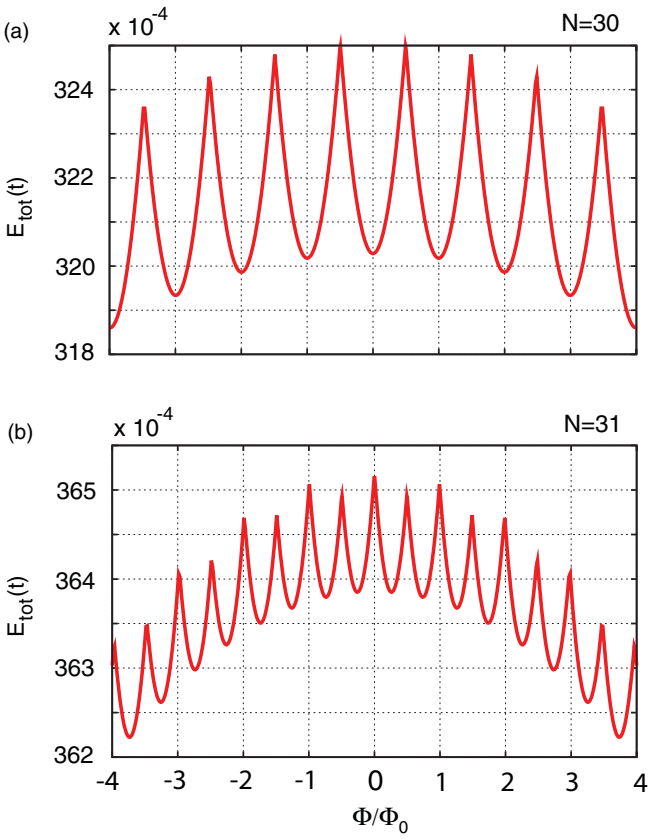

FIG. 6. (Color online) Total energy curves (as a function of the magnetic flux Φ) corresponding to the magnetizations in Figs. 4(b) and 4(c) [case of the thin monolayer hexagonal graphene ring with zigzag terminations portrayed in Fig. 1(b)]. (a) $N = 30$; (b) $N = 31$. Observe the doubling of the frequency and the halving of the amplitude of the oscillations as one goes from $N = 30$ (even) to $N = 31$ (odd).

of this parabolic dependence given the definition of the magnetization as the derivative of the total energy with respect to the magnetic flux [see Eq. (2)].

We have further examined the total energy curves, $E_{\rm tot}^{\rm IMR}(\Phi)$ (not shown here), for the case of an IMR, i.e., using the well-known analytic energies of Eq. (1), and have confirmed that their shape consists of similar parabolic segments exhibiting a Φ_0 or a $\Phi_0/2$ period for even or odd N, respectively.

Naturally, this overall parabolic ($\propto\Phi^2$) dependence of $E_{\rm tot}^{\rm IMR}(\Phi)$ could have been anticipated due to the original parabolic dependence on Φ of the single-particle levels $\varepsilon_i^{\rm IMR}(\Phi)$ [see Eq. (1)]. However, for graphene rings with zigzag terminations, this result is a surprising one, given that the associated single-particle spectrum is much more complicated; it further indicates that the corresponding graphene single-particle energies [associated with the W states; see Secs. III and IV] are parabolic on Φ to a rather large degree.

We further briefly mention here that in preliminary calculations we found that graphene rings with armchair edge terminations have, in contrast to those with zigzag terminations, single-particle spectra with an almost-linear dependence on Φ, and thus their AB patterns are different (as we describe in detail elsewhere).[19]

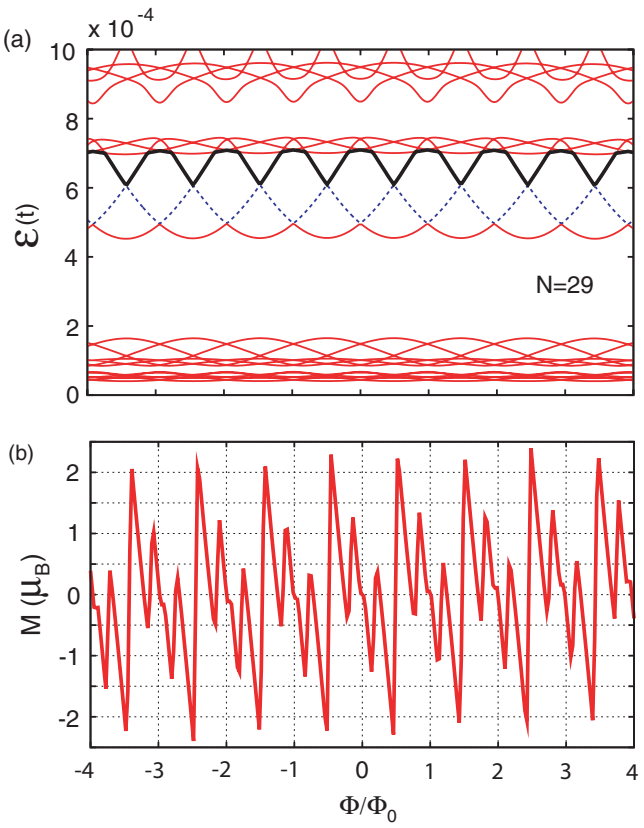

FIG. 7. (Color online) An example of the case of a narrow bilayer hexagonal graphene ring with zigzag terminations on all 12 sides. The bilayer ring is built by stacking (Bernal stacking) two monolayer hexagonal rings resembling the shape in Fig. 1(b). (a) Characteristic part of the spectrum. The thick black line denotes the level occupied by the 29th electron (spin included). The dashed (blue) line denotes the single W state here. (b) Corresponding magnetization curve (for $N = 29$ electrons) as a function of the magnetic flux Φ (spin is included).

VI. BILAYER HEXAGONAL RING

Having addressed the appearance of regular trends in AB oscillations of monolayer graphene nanorings, we comment next on possible modifications that arise in associated bilayer graphene-ring structures. To this end, we consider an hexagonal bilayer ring formed by stacking two monolayer rings [resembling the arrangement portrayed in Fig. 1(b)] one on top of the other following the Bernal prescription. Due to the Bernal-type coupling between the two rings, such narrow bilayer graphene rings are analogs of the double-ring configurations considered recently in the framework of the AB effect in mesoscopic metallic devices.[20]

A characteristic part of the low-energy TB spectra for the bilayer ring is displayed in Fig. 7(a). As was the case for monolayer hexagonal rings, the emergence of sixfold energy bands persists also for the case of a narrow bilayer hexagonal ring. However, the couplings between the layers leads to strong modifications within each energy band; namely, the three top energy levels are strongly compressed compared to the three bottom ones. This results in turn in several more complicated profiles for the AB oscillations, an example of which is displayed in Fig. 7(b). From an inspection of Fig. 7(a), it is also clear that there is only a single well-formed W state that may serve as a Fermi level [see second level from the bottom, denoted by the dashed (blue) line], and thus a halved-period sawtooth pattern occurs only once within the period of 12 electrons (with the spin degeneracy being accounted for).

VII. CONCLUSIONS

Using TB calculations and taking into account the spin, we have demonstrated the universality of the integer (Φ_0) and half-integer ($\Phi_0/2$) magnetic-flux periods in the AB effect in narrow graphene rings with zigzag boundary conditions (trigonal and hexagonal shapes were considered in both monolayer and bilayer structures). The AB patterns for the monolayer hexagonal rings are dominated by an odd-even (in the electron number) alternation of sawtooth-type oscillations with Φ_0 and $\Phi_0/2$ periods. This odd-even alternation persists also for trigonal monolayer and hexagonal bilayer rings, with a reduced occurrence frequency (related to the number of W states in each energy band). Additional patterns of higher complexity are also prominent, depending on the structure of the graphene ring. All AB patterns repeat themselves as a function of N, with periods relating to the point-group symmetry of the geometrical shape of the rings.[21] Our findings, which contrast with the results in recent literature on the subject (see, e.g., Refs. 10 and 11), provide the impetus for experimental probing of AB effects in the graphene systems explored in this paper.

ACKNOWLEDGMENT

This work was supported by the Office of Basic Energy Sciences of the US Department of Energy under Contract No. FG05-86ER45234.

*igor.romanovsky@physics.gatech.edu
†Corresponding author: constantine.yannouleas@physics.gatech.edu
‡uzi.landman@physics.gatech.edu

[1] M. Büttiker, Y. Imry, and R. Landauer, Phys. Lett. A **96**, 365 (1983).
[2] Y. Imry, in *Directions in Condensed Matter Physics*, edited by G. Grinstein and G. Mazenko (World Scientific, Singapore, 1986), p. 101.
[3] H.-F. Cheung, Y. Gefen, E. K. Riedel, and W.-H. Shih, Phys. Rev. B **37**, 6050 (1988).
[4] A. C. Bleszynski-Jayich, W. E. Shanks, B. Peaudecerf, E. Ginossar, F. von Oppen, L. Glazman, and J. G. E. Harris, Science **326**, 272 (2009).
[5] D. Loss and P. Goldbart, Phys. Rev. B **43**, 13762 (1991).

[6]S. Roche, F. Triozon, A. Rubio, and D. Mayou, Phys. Rev. B **64**, 121401(R) (2001); A. Bachtold *et al*., Nature (London) **397**, 673 (1999).

[7]K. S. Novoselov *et al*., Science **306**, 666 (2004).

[8]S. Russo, J. B. Oostinga, D. Wehenkel, H. B. Heersche, S. S. Sobhani, L. M. K. Vandersypen, and A. F. Morpurgo, Phys. Rev. B **77**, 085413 (2008).

[9]M. Huefner, F. Molitor, A. Jacobsen, A. Pioda, Ch. Stampfer, K. Ensslin, and Th. Ihn, New J. Phys. **12**, 043054 (2010).

[10]P. Recher, B. Trauzettel, A. Rycerz, Y. M. Blanter, C. W. J. Beenakker, and A. F. Morpurgo, Phys. Rev. B **76**, 235404 (2007).

[11]C.-H. Yan and L.-F. Wei, J. Phys. Condens. Matter **22**, 295503 (2010).

[12]J. Wurm, M. Wimmer, H. U. Baranger, and K. Richter, Semicond. Sci. Technol. **25**, 034003 (2010).

[13]M. M. Ma and J. W. Ding, Solid State Commun. **150**, 1196 (2010).

[14]Our studies have been motivated by the recent experimental advances concerning the following. (a) The fabrication and engineering of graphene edges with high-purity zigzag terminations: see, e.g., X. Jia *et al*., Science **323**, 1701 (2009); B. Krauss *et al*., Nano Lett. **10**, 4544 (2010); P. Nemes-Incze *et al*., Nano Res. **3**, 110 (2010); R. Yang *et al*., Adv. Mater. **22**, 4014 (2010); Zh. Shi *et al*., *ibid*. **23**, 3061 (2011); J. Lu *et al*., Nature Nanotechnol. **6**, 247 (2011). For the engineering of high-purity armchair edges, see M. Begliarbekov *et al*., Nano Lett. **11**, 4874 (2011). (b) The ability to measure very small magnetic moments and currents: see Ref. 4 and H. Bluhm, N. C. Koshnick, J. A. Bert, M. E. Huber, and K. A. Moler, Phys. Rev. Lett. **102**, 136802 (2009). For a perspective, see Y. Imry, Physics **2**, 24 (2009).

[15]T. Luo, A. P. Iyengar, H. A. Fertig, and L. Brey, Phys. Rev. B **80**, 165310 (2009); H. A. Fertig and L. Brey, Philos. Trans. R. Soc. A **368**, 5483 (2010).

[16]While many-body effects may be of interest in the context of the AB/PC effect for a certain choice of parameters, e.g., when a Wigner molecule is formed [see, e.g., R. Okuyama, M. Eto, and H. Hyuga, Phys. Rev. B **83**, 195311 (2011)], in the current paper we focus on the broad range of instances where the noninteracting electron model provides an appropriate description. In this context, see the experimental study in Ref. 4, where for metal nanorings it was found that "measurements of both a single ring and arrays of rings agree well with calculations based on a model of non-interacting electrons." The results of a recent sole study of many-body effects in graphene rings; [D. S. L. Abergel *et al*., *ibid*. **78**, 193405 (2008)] were obtained, for convenience, with the use of the simplified[15] infinite-mass boundary condition and, consequently are not considered by us here.

[17]R. B. Lehoucq, D. C. Sorensen, and C. Yang, *ARPACK Users' Guide: Solution of Large-Scale Eigenvalue Problems with Implicitly Restarted Arnoldi Methods* (SIAM, Philadelphia, 1998).

[18]D. A. Bahamon, A. L. C. Pereira, and P. A. Schulz, Phys. Rev. B **79**, 125414 (2009) see also Ref. 10.

[19]I. Romanovsky, C. Yannouleas, and U. Landman (to be published).

[20]Y. Avishai and J. M. Luck, J. Phys. A **42**, 175301 (2009).

[21]These patterns are robust with respect to variations in the width of the rings (see, e.g., Fig. 5), as well as to variations in their shape away from a regular polygon (see Ref. 19).